IRAQI JOURNAL OF APPLIED PHYSICS
Vol. 22, No. 2, April-June 2026, pp. 268-280

Sustainable Green Synthesis of Silver Nanoparticles and Carboxymethyl Cellulose Biopolymer and Their UV-Visible Spectroscopic Analysis

Mothana J. Kadhim [1,2*]
Raghad S.A. Al-khafaji [1]

[1] Department of Physics, College of Education/ Ibn Al-Haitham, University of Baghdad, Baghdad, IRAQ
[2] General Directorate of Education/Diyala, Ministry of Education, IRAQ

In this study, orange peels and rice husks were used as agricultural wastes to synthesize silver nanoparticles (AgNPs) in an environmentally friendly and economical manner, using a reducing and capping agent, and to prepare a biopolymer from carboxymethyl cellulose (CMC) nanocomposites with different concentrations (6, 12, 18, 24, 30 and 36%) of silver nanofillers, and hybrid polymer of CMC and polyethylene glycol PEG were prepared. The main vibration peaks of AgNPs and CMC biopolymer were observed, confirming their successful preparation. The AgNPs were found to be spherical and monodisperse. The energy bandgap was reduced from 5.46 eV for pure polymer CMC to 3.43 eV at AgNPs concentration of 36%. This reduction revealed the localized surface plasmon resonance (LSPR) effects, enabling the produced nanocomposite to absorb a broader spectrum of light and improve photocatalytic efficiency.

Keyword: Green synthesis; Optical properties; Carboxymethyl cellulose (CMC); Nanoparticles
Received: 24 July 2025; Revised: 22 October 2025; Accepted: 29 October; Published: 1 April 2026
* Corresponding author email: mothana.jassem1204a@ihcoedu.uobaghdad.edu.iq

1. Introduction

There are several attempts to find an eco-friendly material to address the issues related to plastic waste. The primary agricultural waste products generated during rice cultivation are flour, husk, and straw. About 20% of the 600 million tons of rice produced annually is made up of rice husk (RH), which is unsuitable for use as animal feed due to its high silica content and inability to burn openly or fully degrade. Additionally, RH is composed of 65-75% organic materials (cellulose ,lignin, and hemicellulose) and 15-20% inorganic (SiO_2) [1]. Cellulose, hemicellulose, lignin, L-arabinose, methyl glucuronic acid, D-galactose, and some proteins and vitamins are among the organic components that may be extracted from the rich husk [2].

The most important derivative of cellulose is carboxymethyl cellulose (CMC), which has the ability to act as a strong barrier against lipids, carbon dioxide, and oxygen. It is therefore a crucial ingredient in creating a more resilient film. The CMC has carboxyl (-COO) and hydroxyl (-OH) groups that allow it to interact with positively charged ionic species. The food, detergent, pharmaceutical, textile, paper, paint, and glue industries all make extensive use of CMC cellulose [3]. CMC is a non-toxic biopolymer with excellent biocompatibility and biodegradability. It can be used in contaminant removal applications due to its moderate porosity, active binding sites, and high surface area (108-539 m^2/g) [2,3].

In recent years, the development of nanotechnology has revolutionized, and different metallic nanoparticles have been synthesized using green chemicals instead of external ones that may contaminate the atmosphere [4]. Physical, chemical, electrochemical, sonochemical, irradiation, and biological methods have all been used to create nanoparticles. The biological technique, which uses both phytonanosynthesis (using plants) and microbial nanosynthesis (using microorganisms), is the most favored [5]. Milling and other physical methods of preparing nanoparticles are expensive because they use a lot of energy, and chemical methods are not environmentally friendly because they frequently use hazardous or toxic chemicals as starting materials and release these chemicals into the environment, which damages it [6]. Because harmful agents may be included in the physical or chemical methods of creating nanostructured compounds, in order to reduce or eliminate the use or generation of hazardous substances that have an impact on both human health, the biosynthesis methodology offers a lower cost and a more environmentally friendly procedure [7]. As a result, it is necessary to employ a green synthesis technique, which is a mild and environmentally beneficial way to create nanoparticles by extracting plant components [8]. Noble metal nanoparticles exhibit strong surface plasmon resonance (SPR), which enhances visible light absorption and generates energetic electrons that improve photocatalytic reactions. Embedding these nanoparticles in biopolymer matrices prevents agglomeration,

maintains high surface area, and prolongs the lifetime of charge carriers by facilitating charge separation. The biopolymer's functional groups can also interact with pollutants, improving adsorption and catalytic degradation efficiency under visible light [4].

Studies show that noble metal-biopolymer composites display superior performance in degrading organic dyes and pollutants compared to metal nanoparticles alone or polymers without metal loading. For example, composites of Au or Ag nanoparticles with polymer matrices enhance degradation rates significantly due to increased catalytic active sites and efficient electron transfer pathways. Additionally, biopolymers improve the recyclability and mechanical stability of these composites, making them suitable for repeated use in water treatment applications.

Silver nanoparticles have gained substantial interest due to their appealing physical and chemical characteristics and have been introduced into many polymers [9,10]. PEG helps achieve uniform dispersion of metal nanoparticles within the polymer matrix, preventing agglomeration. It also improves optical properties, such as increased light absorption, scattering, and UV protection. Furthermore, as a polymer matrix, it facilitates better processability via casting, providing flexibility and mechanical support to the composite while maintaining a porous structure. It also helps reduce charge carrier recombination and facilitates efficient electron transfer. All of these features are essential for contaminant adsorption and catalytic reactions [11].

Pure CMC contains only hydroxyl radicals and has low adsorption capacity. Therefore, combining CMC with other functional adsorbents, including silver nanostructure and PEG, can enhance adsorption efficiency by incorporating multifunctional properties into the nanocomposites. Accordingly, the aim of the current study is to disposal of agricultural waste by utilizing it in the green synthesis of silver and CMC and preparing CMC-PEG/AgNPs nanocomposites for optical examinations.

2. Material and Methods

A certain amount of rice husks was obtained from rice mills and washed several times with regular water and then with distilled water and left to dry under the sun for a period of 7 days so that it was completely dry. Then it was ground in a food mill and then sieved with a 75-µm sieve.

The preparation of CMC begins with treating rice husk (RH) in a 6% potassium hydroxide (KOH) solution at 70°C for 1.5 hours, followed by filtering, washing, and drying. The alkaline-treated RH is then mixed with 4% diluted sulfuric acid and stirred at 70°C for another 1.5 hours. Next, the acid-treated RH undergoes bleaching with a 3% sodium chlorite solution at 70°C for 3 hours, during which acetic acid is added to maintain a pH of 3 to 4. The bleached cellulose is subsequently mercerized by treatment with a 20% sodium hydroxide (NaOH) solution in ethanol at 60°C for 1.5 hours. Following mercerization, monochloroacetic acid, in a ratio of 1.2 times the cellulose weight, is added to the mixture and stirred for 1.5 hours to produce CMC. Finally, the CMC is thoroughly washed multiple times with ethanol and methanol before being dried on an electric heater for 48 hours to yield powdered CMC.

The orange peels were collected from Diyala farms in Iraq. It cut into small pieces, then washed with tap water, then distilled water, and left to dry at room temperature for 5-6 days, and then pulverized to a fine powder using grinder. Subsequently, it passed through a 75-µm sieve. The extract was prepared with percent 1:6 (w/v) of ground orange peels to deionized water, then dissolving them for two hours, followed filtering it with filter paper three times, then placing it in a clean bottle in the refrigerator until use.

A magnetic stirrer was used to dissolve 20 g of silver nitrate ($AgNO_3$) in 75 ml of distilled water at 50°C while stirring continuously for 15 min. After that, 50 ml of orange peel extract was distilled into the solution drop by drop while being constantly stirred, and the temperature was raised to 70°C. A change in the solution's hue was seen following the distillation of the extract solution, where the solution turns darkish red brown. NaOH solution 0.1 M was added for adjusted pH value around 7 to 8. Centrifugation was used to separate the precipitate and the resulting powder was then washed with ethanol five times using a centrifuge. Silver nanoparticles were obtained by drying the precipitate for an hour at 70°C in an oven. Then the silver was calcined at 300°C for one hour, to remove residual organic materials.

The CMC-PEG/Ag nanocomposite was prepared by casting method, where AgNPs mixing with CMC and PEG in different proportions as shown in table (1), after dissolving each of them separately in 30 ml of DI distilled water at 70°C for approximately 5 hours. Furthermore, adding citric acid monohydrate at a rate of 15% of the total weight of solid sample for the purpose of crosslinking the materials together [10]. The previous steps were repeated without adding silver nanoparticles to sample A0. The homogeneous polymer nanocomposite mixture was poured into glass molds and allowed to air dry and then oven-cured for two hours at a temperature 80°C that increased the mechanical bonding between the materials. The resulting powder was ground and screened at 50 µm.

3. Characterizations

The nanocomposites manufactured by incorporating silver nanofillers into CMC/PEG blends were characterized by FTIR and UV-visible spectroscopy to identify their different optical properties for potential use in photocatalysis.

Fourier-transform infrared (FTIR) spectroscopy was used to determine which functional groups were present in each nanoparticle. The boundary construction of the resulting samples with an absorption range of 500-4000 cm^{-1} was analyzed using the FTIR spectrum (Frontier FTIR 88091). The morphology of Ag nanoparticles (as-prepared and after calcination), CMC, A0 and A6 were examined using field-emission scanning electron microscopy (FE-SEM) (FEI Company Inspect S50) combined with an X-ray (Flash 6l10 Model, Burker Company, Germany).

Table (1) The material ratios and weights in the preparation of nanocomposites

Sample Code	Ag (Wt.%)	CMC (Wt.%)	PEG (Wt.%)
A0	0	60	40
A1	6	60	34
A2	12	60	28
A3	18	60	22
A4	24	60	16
A5	30	60	10
A6	36	60	4

The optical characteristics of AgNPs, CMC and CMC-PEG/Ag nanocomposites synthesized by the green approach are assessed at room temperature within 200-1000 nm using Shimadzu, UV-1800 UV–visible spectrophotometer. A 10 mg of the solution was dissolved in 5 ml of deionized water and then dispersed in an ultrasonicator for 30 min. The solution was then placed in a quartz optical cuvette with a path length of 1 cm. This procedure was applied for all above samples.

The chemical bonds and functional groups of the AgNPs and CMC were examined using FTIR spectroscopy in the range of 500-4000 cm^{-1}, as seen in Fig. (1). Table (2) shows the summary of FTIR spectral data for the preparation of both AgNPs using orange peel extract and CMC derived from rice husks (RH).

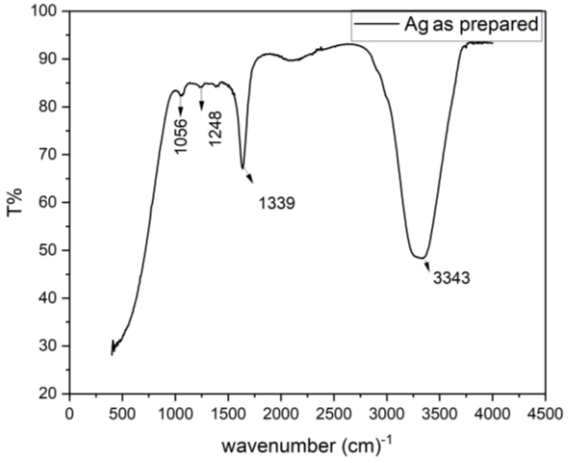

(a)

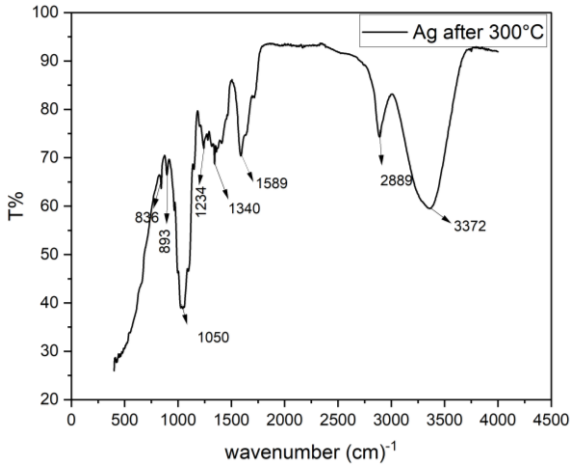

(b)

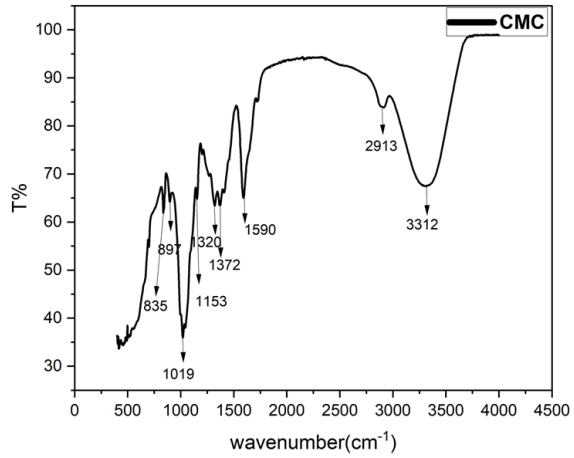

(c)

Fig. (1) FTIR analysis for the (a) AgNPs before and (b) after calcination and (c) CMC polymer

The existence of produced silver nanoparticles (AgNPs) is confirmed by the FTIR spectrum as shown in Fig. (1b). A broad peak is observed around 3343 cm^{-1} due to O–H and N-H stretching vibrations of phenols, amines and alcohol groups from plant biomolecules or residual moisture or hydroxyl groups adsorbed on the surface. The C-H band of the stretching vibration of the aliphatic hydrocarbon chains, which originates from either the methylene or methyl group of the lipids in the orange peel extract, is responsible for the band at 2889 cm^{-1} [11]. The stretching vibration of the olefinic double bond (C=C) corresponds to unsaturated fatty acids and aromatic compounds which represented by the band at 1637 cm^{-1} [12]. The peaks at 1248 and 1234 cm^{-1} are corresponding to the stretching vibrations of C=O and C-N from alcohols, ethers, and amines. The band 1340 cm^{-1} caused by the bending vibrations of OH, the 893 cm^{-1} band corresponding to the bending vibrations of C=C [13]. The process of dumping silver ions onto silver metal may include these biomolecules. The large quantity of phenol that served as a reducing agent for Ag^{+} to Ag^{0} in the creation of AgNPs is confirmed by the larger peak seen at 3372 cm^{-1}.

Flavonoids, alkaloids, tannins, and essential oils are all present in these phenol rings in orange peel extract. Where, an enol of a phenolic molecule releases its electron. Ag^+ is reduced to Ag^0, the silver nanoparticle, by the electron released when the H from the OH bond breaks [11,14]. In FTIR spectrum after calcination at 300°C for one hour, the intensity of the broad O-H peak around 3372 cm^{-1} reduces, indicating loss of hydroxyl groups due to thermal degradation of organic molecules. Peaks around 1600-1000 cm^{-1} which assigned to organic functional groups such as C-H, C-C, C-O, N-H and C-N decreased, signaling decomposition of capping biomolecules. Strong, sharper peaks near 500 cm^{-1} correspond to Ag–O stretching vibrations, which may become more prominent or better resolved due to removal of organics. The most diagnostic area in FTIR is between 1500 and 1800 cm^{-1}. In this area, fibrous cellulose hardly has any peaks; instead. Figure (1c) shows the CMC spectrum, a peak at 1590 cm^{-1}, which corresponds to the carboxylate C=O stretching [14]. The hydroxyl (OH) group stretching frequency was indicated by the wide peak at 3312 cm^{-1}, whilst the (CH) stretching vibration represent carboxymethyl group (CH_2) was responsible for the peak at 2913 cm^{-1}, the 1372 cm^{-1} band caused by the bending vibrations of O-H. According to the literature, the peaks at 1590 and 1372 cm^{-1} reveal certain features of CMC [3]. The peaks at 1153 and 887 cm^{-1} are corresponding to the stretching vibration of C=O and bending vibrations of C=C [15].

FE-SEM images in Fig. (2a) for CMC show the particles appear as varying-sized fragments with some appearing flattened or sheet-like, which suggests the breakdown of native structures during the derivatization process where introduces carboxymethyl groups into the cellulose structure. Also exhibit, a pronounced porous smooth morphology in the CMC films. The chemical process breaks down and removes considerable portions of lignin, hemicellulose, and silica, leading to a more open and porous polymeric matrix.

The resulting porous structure features micro- to nanoscale pores formed by polymer chain entanglement, increased hydrophilicity from introduced carboxymethyl groups, and swelling, which enhances water absorption and diffusion properties, significantly surface reactivity. These correlate with enhanced photocatalytic efficiency for wastewater purification application.

Based on FE-SEM images displayed in Fig. (2b), the morphology of the synthesized silver nanoparticles (AgNPs) exhibits characteristic features reflecting the influence of bio-reducing and capping agents derived from the peel. The silver nanoparticles have a regular spherical shape, and smooth indicating isotropic growth, which suggests that the biomolecules in the orange peel extract (proteins, flavonoids, and phenolic compounds) act as reducing and stabilizing agents. The particles also appear uniform in size and shape, suggesting a controlled nucleation and growth process. The presence of homogeneity indicates effective stabilization by phytochemicals, preventing excessive agglomeration and allowing for consistent particle formation. As well as, the nanoparticles appear well dispersed with minimal aggregation, confirming the role of coating agents in providing steric or electrostatic stabilization and maintaining colloidal stability.

The observed particle crystal sizes range between 33-37 nm. This indicates the appropriate synthesis conditions (pH, temperature, extract concentration, reaction time). Figure (2c) exhibit AgNPs calcined at 300°C lead to increased crystallinity, homogeneity and larger particle sizes range between 60-70 nm.

Micrograph in figures (2d) and (2e) appear the addition of PEG to the CMC matrix enhances the membrane's flexibility by reducing crystallinity and disrupting the rigid CMC chain cohesion. Hydrogen bonding between CMC and PEG promotes good miscibility and polymer chain entanglement, which is observed as a uniform phase in FE-SEM without significant phase segregation or aggregation. This also results in a significant reduction in surface defects, such as cracks or pores. The particle size distribution histogram using ImageJ software. The energy-dispersive X-ray spectroscopy (EDX) reveals strong signal in the silver region and confirms the formation of silver nanoparticles. The EDX spectra of a sample CMC where the peaks of oxygen and carbon appear as the main elements, which make up cellulose.

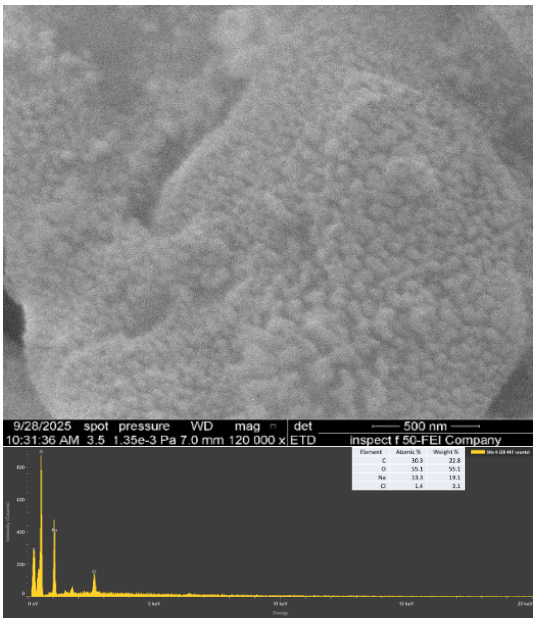

(a) CMC

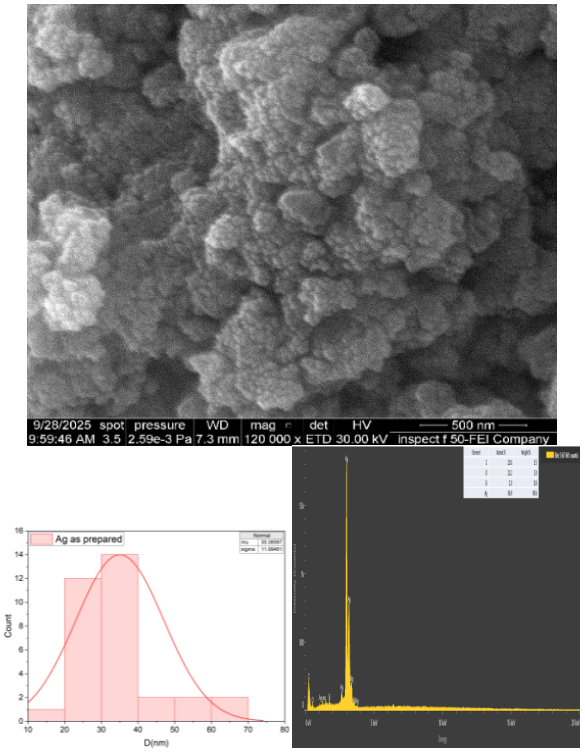

(b) As-prepared AgNPs

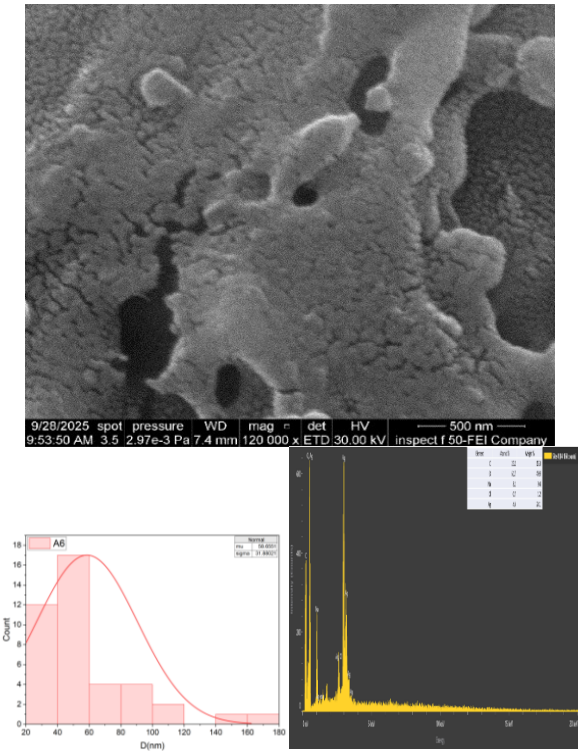

(d) A6 sample

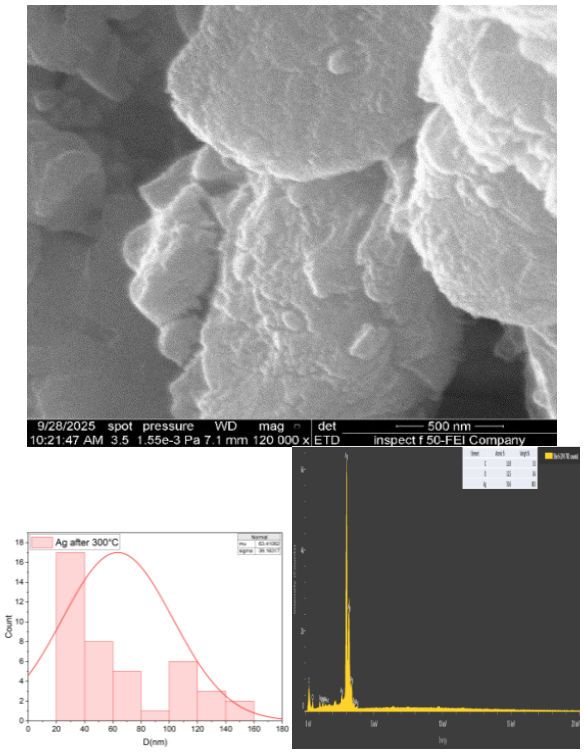

(c) AgNPs after calcination

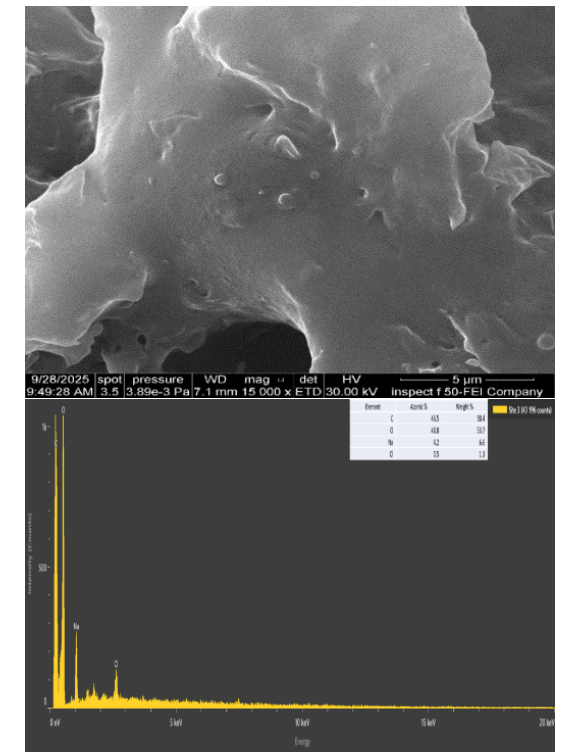

(e) A0 sample

Fig. (2) FE-SEM images of (a) CMC, (b) as-prepared AgNPs, (c) AgNPs after calcination, (d) A6 sample, (e) A0 sample, (f) Particle size distribution histogram, and (c) EDX spectra for elemental composition

UV-visible absorption spectroscopy is a useful method for characterizing the band gap and absorbance bands of nanoparticles, particularly noble metals,

which exhibit absorptions from surface plasmon oscillations and are highly colored. Light waves that interact with the metal's free electrons and become trapped on the surface are known as surface plasmons. Interestingly, the SPR band is exclusive to metal nanoparticles and does not appear in the spectrum of their bulk counterparts [16]. In general, the surface plasma resonance phenomenon causes silver nanoparticles to show significant absorption in the UV-visible range. Silver nanoparticles are most frequently seen at UV wavelengths, when the so-called "surface plasmon absorption band" is visible. The detection of silver nanoparticles in colloidal solution was made possible using UV-visible absorption spectroscopy. This mainly happens for tiny spherical silver nanoparticles in the 380-450 nm range [17].

The transmittance (T), which is given by the Beer-Lambert law, is the ratio of the incident light intensity (I_0) to the transmitted light intensity (I_t) as [18]

$$T = \frac{I_t}{I_0} = 10^{-A} \quad (1)$$

However, as the absorbance (A) represents the negative logarithm of transmittance (T), known as the optical density, and may be expressed as follows [18]:

$$A = \text{Log } T^{-1} \quad (2)$$

The reflectance (R) can be estimated using the following formula:

$$R = 1 - A - T \quad (3)$$

It is clear from Fig. (3a**)** that the produced AgNPs' SPR peaks were detected at about 400 and 420nm before and after calcination, respectively. The wavelength of the nano silver shifts towards the visible light (red shift) after calcining it at 300°C referred to changes in the color of the samples from (yellow to darkish red brown) as prepared and from (black to light brown) after calcination which indicates the presence of well-dispersed AgNPs with characteristic SPR absorption. Calcination process provides thermal energy that promotes particle growth and crystallinity, leading to a shift of the SPR peak towards longer wavelengths, as observed in various studies [20,21]. As silver nanoparticles were synthesized using plant extracts, the spectrum results demonstrated the plant's suitability (orange peel extract) for producing nanomaterials by reduction the concentration of silver ions Ag^+ into Ag^0 in solution, the synthesis was initially confirmed by the change in color of the silver nitrate solution from transparent to reddish brown when the orange peel extract was distilled. It was discovered from Fig. (3c) that the absorbance of the whole nanocomposites drops as the wavelength increases. Because the incident photon's energy is smaller than the nanocomposite energy gap, it is physically impossible for it to excite an electron and transfer it from the valence band to the conduction band. Additionally, it is evident that as the proportion of AgNPs filling rises, so does the absorbance due to increased surface plasmon resonance effects where creating localized levels inside the energy gap, which in turn caused the absorption of low-energy photons, this validates the entrance of silver into the prepared sample's crystal structure, from these results, these CMC-PEG/Ag nanocomposites can act as photocatalysts in the UV and visible region.

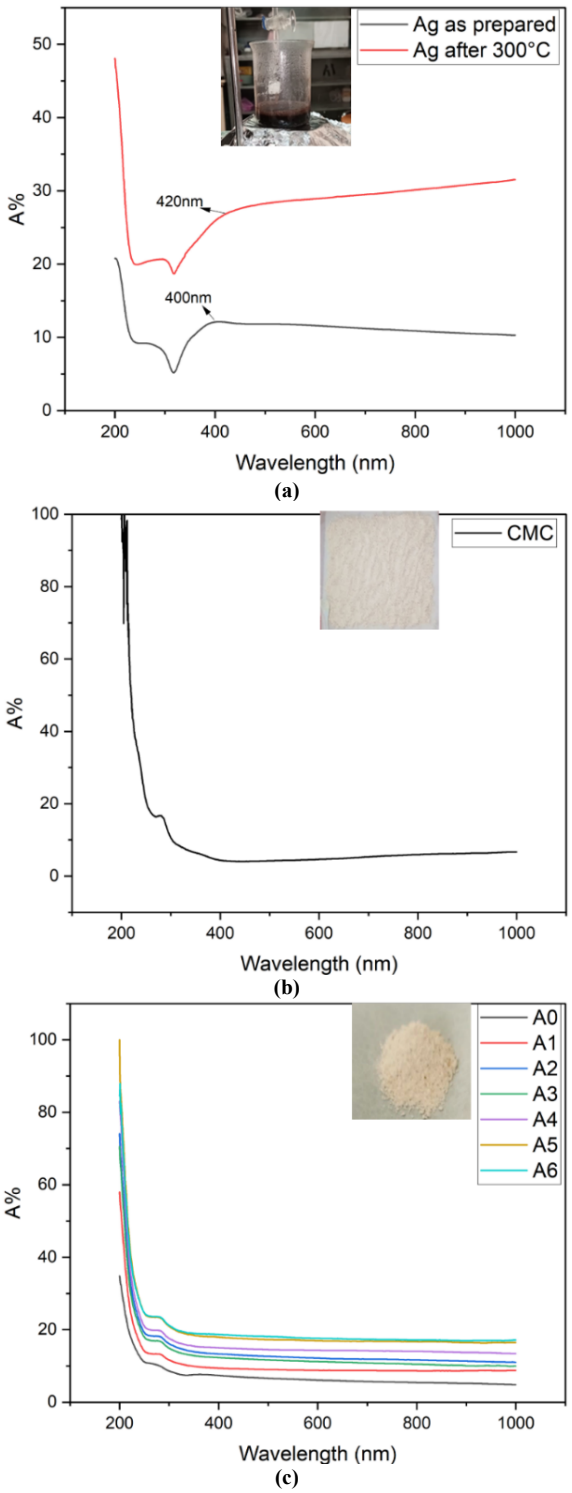

Fig. (3) Absorption spectra of prepared samples as a function of wavelength for (a) AgNPs, (b) CMC and (c) CMC-PEG/Ag nanocomposites

From the absorbance results, the transmittance was calculated according to Eq. (1), before calcination, AgNPs have a greater transmittance than nano silver after calcination. Because transmittance and absorbance have an inverse relationship. The transmittance spectra of the CMC-PEG/Ag nanocomposites are displayed in Fig. (4c). The transmittance of the nanocomposite is affected by a variety of factors, including intrinsic material properties such as particle size and refractive index of the components, as well as composite fabrication factors such as nanocomposite filler concentration, surface roughness, and particle dispersion state. Thus, particles with sizes larger than the visible wavelength would obstruct light, leading to transparency or opacity. Due to the absence of light-blocking particles, the pure CMC blend A0 has the highest percent transmittance. As the nanoparticle content increases, the optical density of the nanocomposite rises, resulting in more significant absorption and scattering of incident light, which diminishes transmittance [22].

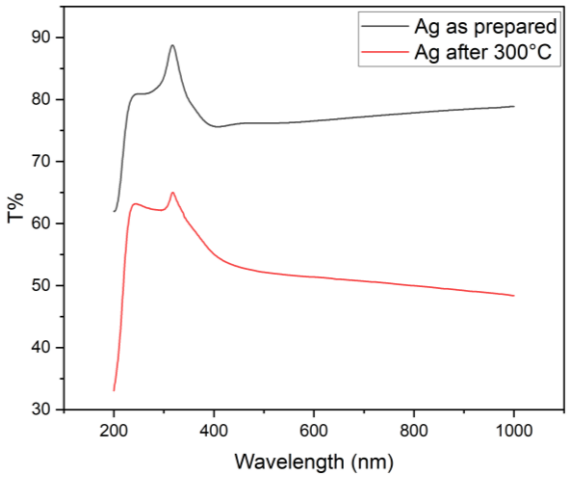

(a)

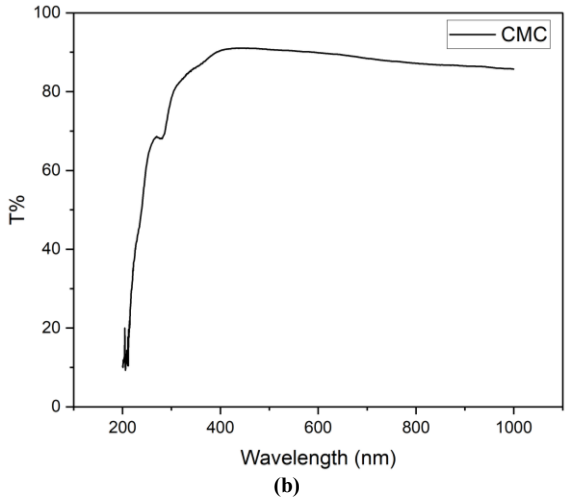

(b)

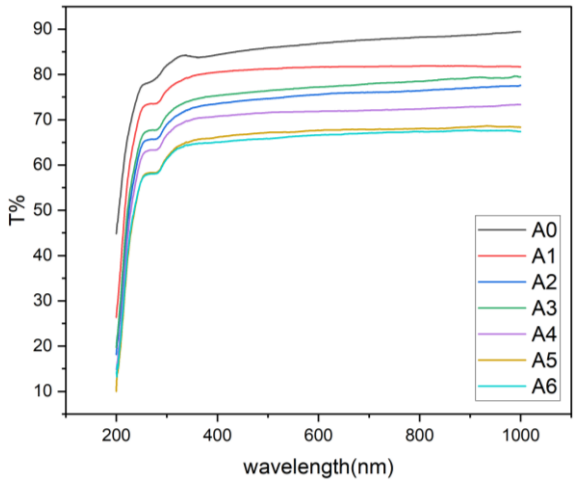

(c)

Fig. (4) Transmission spectra (T) of (a) AgNPs, (b) CMC and (c) CMC-PEG/Ag nanocomposites

The reflectance (R) was calculated from the absorption and transmission spectra according to Eq. (3). Figure (5) shows the reflectance as a function of wavelength for AgNPs, CMC, and CMC-PEG/Ag nanocomposites. It is evident from Fig. (5c) that the reflectance of the CMC-PEG/Ag nanocomposites increase with increasing wavelength for short wavelengths (200-350nm), while for long wavelengths (350-1000nm), the reflectance decreases with increasing wavelength. With increasing weight percentage (wt.%) of AgNPs fillers, the reflectance increases for all wavelengths [23].

The amount of energy absorbed by the sample, or the extinction of electromagnetic waves within the material, is known as the extinction coefficient (K). It is determined by the following relation [18]

$$K = \frac{\alpha\lambda}{4\pi} \qquad (4)$$

where λ is the wavelength and α is the absorption coefficient, which can be calculated from the following relation [24]

$$\alpha = (2.303\,\frac{I_0}{I})/d = (2.303A)/d \qquad (5)$$

where A is the absorbance and d is the sample thickness, which is equal to the width of the cuvette (d=1cm)

The extinction coefficient changes for prepared AgNPs, CMC, and CMC-PEG/Ag as a function of wavelength is displayed in figures (6a), (6b) and (6c), respectively. At short wavelengths (200-350nm), the extinction coefficient becomes less prominent, whereas it becomes more apparent in the visible and near-infrared spectra (350-1000nm). Since the extinction coefficient and the absorption coefficient are related, an increase in the absorption coefficient also results in an increase in the extinction coefficient.

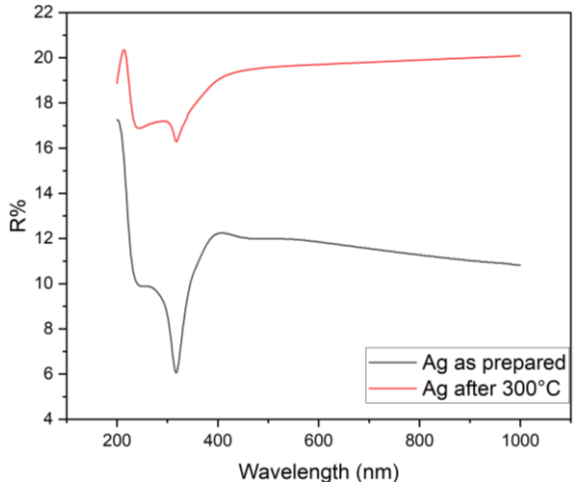

(a)

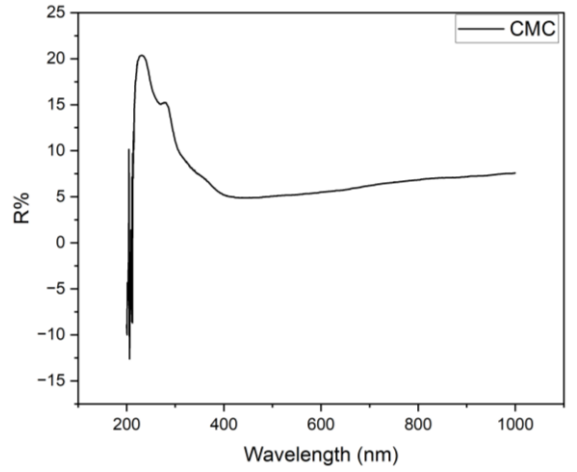

(b)

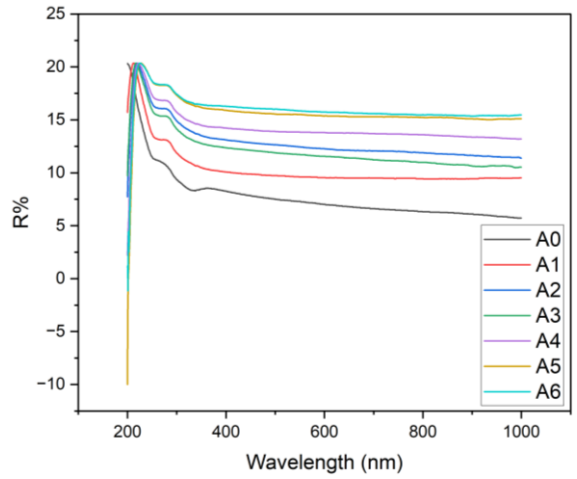

(c)

Fig. (5) The reflection spectra (R) of (a) AgNPs, (b) CMC and (c) (CMC-PEG/Ag) nanocomposites

It can be observed from these data that the extinction coefficient increases with wavelength, and the AgNPs, CMC, and produced CMC-PEG/Ag do not exhibit a considerable attenuation in the low wavelength region. Besides, the extinction coefficient of the CMC-PEG/Ag nanocomposites are displayed in Fig. (6c). As the percentage of AgNPs filling increases, the nanocomposite's extinction coefficient rises. The extinction coefficient for CMC-PEG/Ag nanocomposites were larger in concentrations (36 wt.% AgNPs) and lower extinction coefficient at (6 wt.% AgNPs). Therefore, the extinction coefficient for nanocomposites increases with the increase of filler of AgNPs as a result of the increase in the absorption coefficient, that mean increase the amount of energy lost during the electromagnetic wave's passage through the substance [25].

The refractive index of all produced AgNPs, CMC and CMC-PEG/Ag nanocomposites, shown in Figs. (7a), (7b) and (7c), respectively, was calculated within wavelength range of 200-1000 nm. The following relation may be used to estimate the refractive index [19]

$$n = \sqrt{\left(\frac{1+R}{1-R}\right)^2 - (K^2+1)} + \frac{1+R}{1-R} \qquad (6)$$

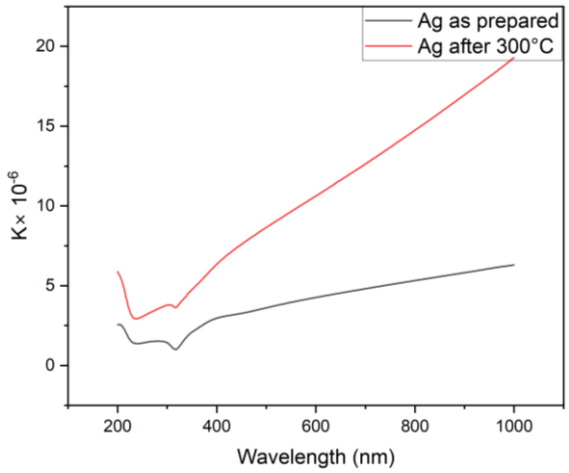

(a)

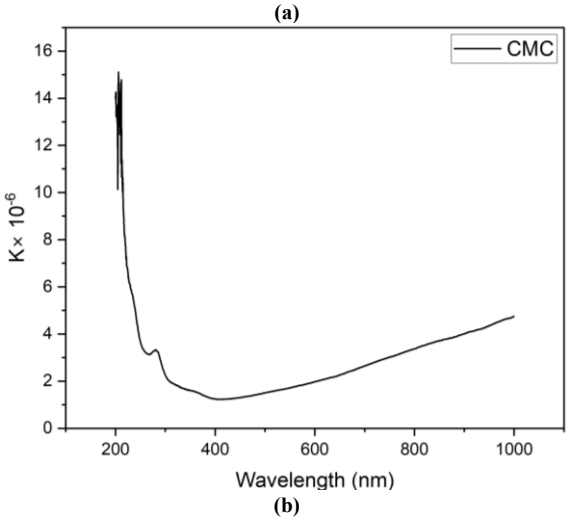

(b)

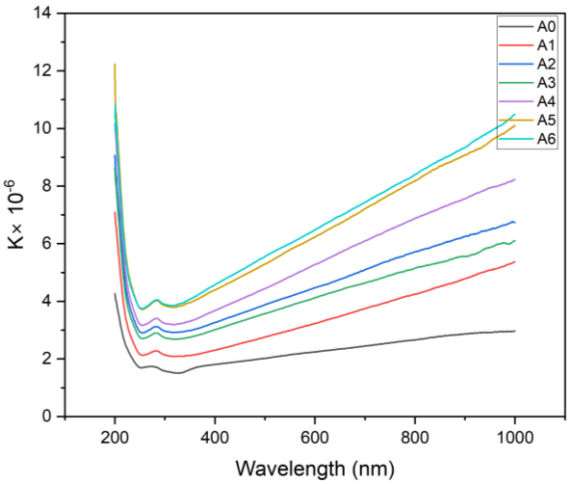

(c)

Fig. (6) Extinction coefficient (K) for (a) AgNPs, (b) CMC and (c) CMC-PEG/Ag nanocomposites

As can be seen from the Fig. (7a), the refractive index at wavelengths 400 and 420nm is n=2 and n=2.5 for AgNPs before and after calcination, respectively, as reported in previous research [26]. The calcination of AgNPs improves crystallization, which raises the material's visual density and raises the refraction parameter of AgNPs. Following calcification, a reduction in the energy gap was also noted, improving the material's capacity to interact with light. These modifications show that the calcination is a useful tool for improving the visual characteristics of the AgNPs [27]. From the Fig. (7b) the maximum value of the refractive index of CMC is n=2.6 at wavelength of 227 nm as mentioned in previous research [28]. Figure (7c) shows that the refractive index increases with increasing weight percentages of AgNPs in the polymer matrix (CMC/PEG), where the highest value shows at wavelength of 280 nm is n=2.5 the ratio of 36 wt.% AgNPs, while the lowest value is n=2.1 at the same wavelength for the ratio of 6 wt.% AgNPs, this is due to the improvement in the density of the nanocomposite as a result of the interaction of AgNPs with the polymer chains, which leads to a change in the distance between atoms within the polymer molecules and in the hydrogen bonds that form between the OH groups on the surface of the AgNPs particles and the OH groups of the CMC/PEG molecules [29].

PEG, a polymer with high molecular weight and specific dielectric properties, it increases the overall polarizability. As a result, the total optical density of the increases, leading to a higher refractive index as present in sample A0.

The high refractive index increases the nanocomposite's ability to bend incident light and trap it within the material. This enhances light absorption efficiency, allowing more photons to interact with the photocatalyst, thus enhancing its photocatalytic activity [16,18].

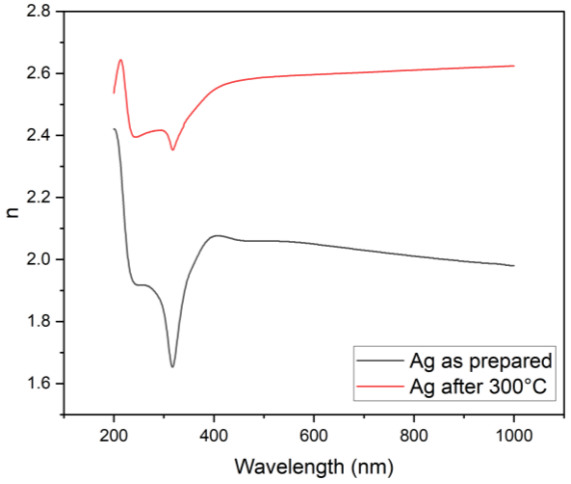

(a)

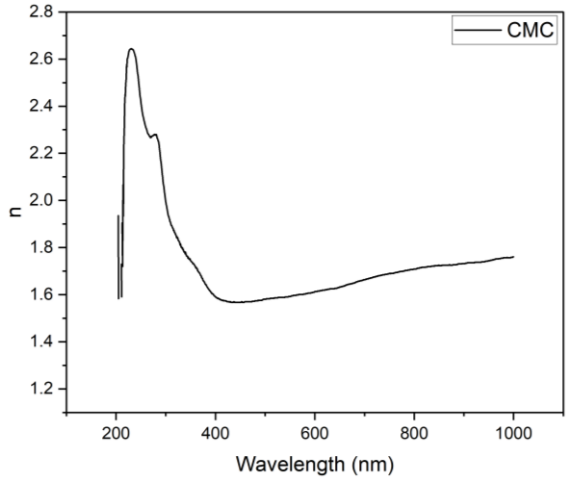

(b)

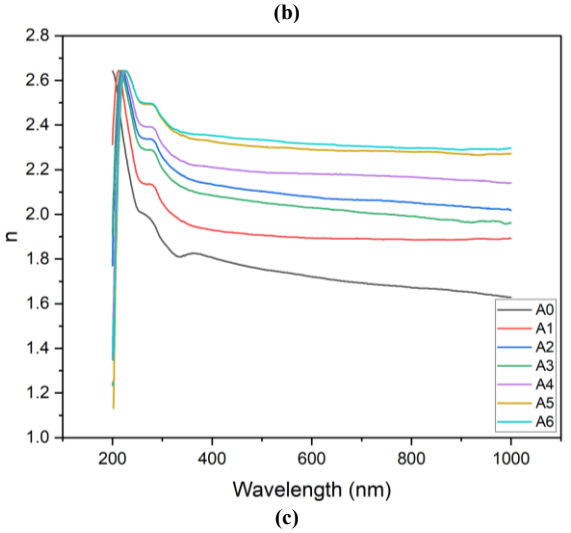

(c)

Fig. (7) The refractive index as a function of wavelength for (a) AgNPs, (b) CMC and (c) CMC-PEG/Ag nanocomposites

The data were utilized as an input to create the algorithms that determine the energy band gap using the Tauc's relation as shown in Eq. (7) [30]

$$(\alpha h\nu) = \beta\,(h\nu - E_g)^n \qquad (7)$$

where β is a constant, E_g is the optical bandgap in electron volts (eV), n is an exponent that can have a

variety of values based on the type of electronic transition, such as n = 2 for direct transitions and n = 1/2 for indirect transitions, and h is the incident photon energy. The absorption coefficient may be used to calculate the optical band gap. Plotting $(\alpha hv)^2$ on the y-axis versus (hv) on the x-axis allows us to determine the direct and indirect optical energy gap [31]. From UV-visible spectrum it can be locate the onset of absorption – the point where the absorption coefficient starts to increase sharply, indicating the transition region. This is typically near the absorption edge associated with the band gap. Focusing on the linear portion of the plot near the absorption edge, where a tangent line is drawn and extended until it intersects the energy axis. The intersection point gives an estimate of the band gap energy.

Green or eco-friendly formulations are significant because of their enormous photocatalytic potential. The plant extract (orange peel) contains proteins, flavonoids, and phenols that are crucial to the stability and environmentally friendly manufacturing of AgNPs with resulted energy gap as shown in Fig. (8a) (3.1 and 2.5 eV) before and after calcination respectively [14,32]. Nanoparticles have a high adsorption capacity to be utilized in photocatalysis to purify water. From table (3) and Fig. (8b), it is clear that the energy gap of prepared CMC is equal to 5.46 eV [28]. Because it is hydrophilic, CMC's presence as a supporting biopolymer matrix guarantees the stability and excellent diffusion of AgNPs inside the polymer matrix, increasing the interaction between AgNPs and water contaminants. Furthermore, because of its negative charge, CMC is an efficient biopolymer that greatly aids in the adsorption process of contaminants found in contaminated water [33]. It is evident from Fig. (8c), that the pure polymer mixture's (CMC-PEG) energy gap was 5.02 eV this result is almost consistent with the result of the previous study [34]. Nevertheless, reinforcement with silver nanoparticles (AgNPs), we observed that the energy gap values generally started to progressively reduce as the amount of additional silver nanoparticles increased. This decrease in energy gap values is explained by a shift in the optical energy levels' positions, which makes it easier for electrons to move from the valence band to the conduction band because the potential barrier between them is lower. This makes it easier for charge carriers to move between the two local levels. Electronic conductivity is dependent on the reinforcement ratios and the availability of an increase in the percentage of added nanoparticles in the formation of electronic paths in the polymer (CMC-PEG), which facilitate the passage of electrons from the valence band to the conduction band, as it is thought to be responsible for the formation of some local defects within nanocomposites [34]. Figure (8c) and table (3) show that the lowest value of the energy gap was 3.74 eV at the ratio of 6 wt.% AgNPs. As the percentage of AgNPs particles in the polymer mixture increases, the optical energy gap values decrease until the value drops to 3.43 eV for the ratio of 36 wt.% AgNPs.

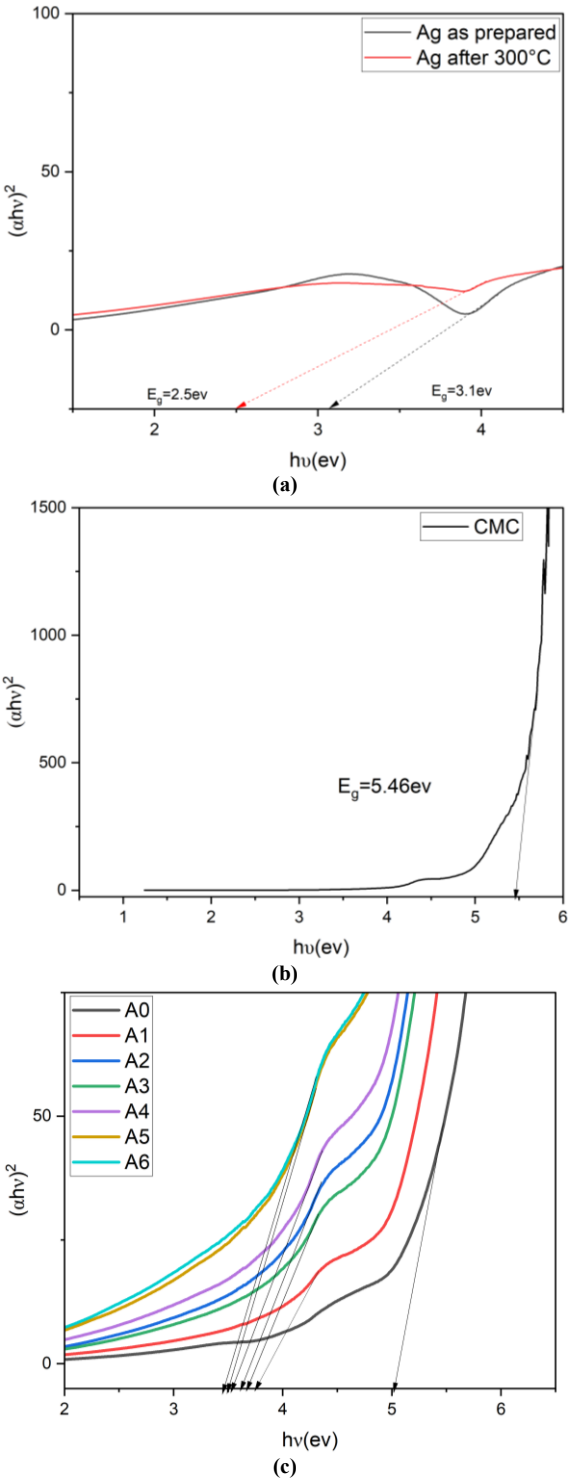

Fig. (8) Determination of the direct optical energy gap for (a) AgNPs, (b) CMC and (c) CMC-PEG/Ag nanocomposites

Table (3) The direct optical energy gap for AgNPs and nanocomposites

Sample Code	E_g (eV)
As-prepared AgNPs	3.10
AgNPs after calcination 300°C	2.50
CMC	5.46
A0	5.02
A1	3.74
A2	3.67
A3	3.61
A4	3.54
A5	3.50
A6	3.43

As well, PEG molecules can influence the electronic environment within the polymer matrix. By incorporating PEG, the interatomic and intermolecular interactions are altered, which can affect the way electrons are excited across the energy levels. This directly impacts the optical energy band gap [11,18]. At this range of energy gap, which falls within the visible spectrum, this nanocomposites can work as a photocatalyst and be invested in the technology of removing pollutants from polluted water, as the electron (e^-) from the nanocomposite's valence band (VB) will be photoexcited to the empty conduction band (CB) in femtoseconds upon exposure to light, leaving a hole (h^+) in the (VB) of the nanocomposite. Transferred to the photocatalyst surface, this (e^-/h^+) pair (charge carriers) takes part in the oxidation and reduction processes, (ROS) which the main weapons that cause photocatalytic activity where has the ability to decompose pollutants present in water [35].

4. Conclusion

Silver nanoparticles (AgNPs) were successfully synthesized through a green approach and incorporated into a biopolymer matrix CMC derived from agricultural waste, besides PEG as plasticizer. The resulting nanocomposites exhibited significant modifications in their optical properties, notably an increase in refractive index and a decrease in band gap energy with rising nanoparticles content. The band gap narrowing, attributed to the localized surface plasmon resonance (LSPR) effects of AgNPs, extends the nanocomposite's photoresponse into the visible spectrum. Which improved photocatalytic performance, demonstrates the potential of sustainable, biopolymer-based nanocomposites incorporating green-synthesized metallic nanoparticles, aligning with principles of green chemistry, as efficient, eco-friendly solutions for water purification and environmental remediation.

References

[1] P.U. Nzereogu et al., "Silica extraction from rice husk: Comprehensive review and applications", *Hybrid Adv.*, 4 (2023) 100111.

[2] S. Kumar et al., "Utilization of Rice Husk and Their Ash : A Review", *J. Chem. Environ. Sci.*, 1(5) (2013) 126-129.

[3] R. Singh, J. Singh and H. Singh, "Green synthesis of carboxymethyl cellulose from agricultural waste its characterization", *J. Phys.: Conf. Ser.*, (2022) 12144.

[4] A.L. Scutaru et al., "Comparative Study on the Influence of Noble Metal Nanoparticles (Ag, Au, Pd) on the Photocatalytic Activity of ZnO NPs Embedded in Renewable Castor Oil Polymer Matrices,", *Materials (Basel)*, 13(16) (2020) 3468.

[5] M. Karem and R. Al-Khafaji, "Microstructure and Morphology of CuAg/Pbo Nanoparticles Synthesized by Pulsed PLAL", *Sci. Int.*, 30 (2018) 829-835.

[6] L. Mogole et al., "Green synthesis of silver nanoparticles using aqueous extract of Citrus sinensis peels and evaluation of their antibacterial efficacy", *Green Process. Synthes.*, 10(1) (2021) 851-859.

[7] K.A. Jasim and R.S. Al-Khafaji, "The effect of oxygen flow on the transition temperature of $Hg_{0.75}Pb_{0.25}Sr_{2-y}Ba_yCa_2Cu_3O_{8+\delta}$ superconductors", *J. Phys.: Conf. Ser.*, (2018) 12096.

[8] A.A. Fayyadh and M.H.J. Alzubaidy, "Green-synthesis of Ag_2O nanoparticles for antimicrobial assays", *J. Mech. Behav. Mater.*, 30(1) (2021) 228-236.

[9] R.S.A. Al-Khafaji, "Synthesis and some features of three-phases polymer/metal/ceramic multilayers nanocomposite", *Ibn AL-Haitham J. Pure Appl. Sci.*, 33(4) (2020) 10-17.

[10] K.K. Mali et al., "Citric Acid Crosslinked Carboxymethyl Cellulose-based Composite Hydrogel Films for Drug Delivery", *Indian J. Pharmaceut. Sci.*, 80(4) (2018) 657-667.

[11] R.L. Jawad and R.S. Abbas, "Formation of Titanium Dioxide by Hydrolysis Catalyst: Effect of Calcination Temperature on Microstructure Characteristics of Polymeric Nanocomposites", *Petrol. Chem.*, 65 (2025) 566-575.

[12] J.A. Abdullah, M.J. Rosado and A.G. Alberto Romero, "Effect of Calcination Temperature and Time on the Synthesis of Iron Oxide Nanoparticles: Green vs. Chemical Method", *Materials (Basel)*, 16(5) (2023) 1798.

[13] R.S.A. Al-Khafaji, "Synthesis of blend polymer (PVA/PANI)/Copper (1) oxide nanocomposite: thermal analysis and UV-Vis spectra specifications", *Iraqi J. Sci.*, 62(11) (2021) 3888-3900.

[14] A.S. Gungure et al., "Studying the properties of green synthesized silver oxide nanoparticles in the application of organic dye degradation under visible light", *Sci. Rep.*, 14(1) (2024) 26967.

[15] S. Rashid and H. Dutta, "Physicochemical

characterization of carboxymethyl cellulose from differently sized rice husks and application as cake additive", *LWT*, 154 (2022) 112630.

[16] S.M. Ismail and S.M. Ahmed, "The Effect of Calcination Temperatures on the Properties of ZnO Nanoparticles Synthesized by Using Leaves Extracts of Pinus Brutia Tree", *Science J. Univ. Zakho*, 11(2) (2023) 286-297.

[17] A. Ajaypraveenkumar et al., "Characterisation, Luminescence and Antibacterial Properties of Stable AgNPs Synthesised from AgCl by Precipitation Method", *J. Mater. Sci. Technol.*, 31(11) (2015) 1125-1132.

[18] R.L. Jawad and R.S. Abbas, "Preparation of titanium dioxide NPs and study of optical parameters as a polymer photocatalytic film", *J. Theor. Appl. Phys.*, 18 (2024) 1-10, doi: 10.57647/j.jtap.2024.si-AICIS23.11.

[19] B.H. Hussein and H.K. Mahmood, "Preparation and Study Annealing Effect on Structure and Optical Properties of $ZnIn_2(Se_{0.8}Te_{0.2})_4$ Thin Film", *Ibn AL-Haitham J. Pure Appl. Sci.*, 38(1) (2025) 174-185.

[20] P. Pandey et al., "Effect of annealing temperature on morphological and optical transition of silver nanoparticles on c-plane sapphire", *J. Nanosci. Nanotechnol.*, 18(5) (2018) 3466-3477.

[21] C. Durucan and B. Akkopru, "Effect of calcination on microstructure and antibacterial activity of silver- containing silica coatings", *J. Biomed. Mater. Res. Part B: Appl. Biomater.*, 93(2) (2010) 448-458.

[22] K.M. Abu Hurayra–Lizu et al., "GO based PVA nanocomposites: tailoring of optical and structural properties of PVA with low percentage of GO nanofillers", *Heliyon*, 7(5) (2021) e06983.

[23] S. Rafique et al., "Fabrication of silver-doped zinc oxide nanorods piezoelectric nanogenerator on cotton fabric to utilize and optimize the charging system", *Nanomater. Nanotechnol.*, 10 (2020), doi: 10.1177/1847980419895741.

[24] R.L. Jawad and R.S. Abbas, "Exploring the Variation of Urbach Energies Between Anatase and Rutile Phases of TiO_2 Nanoparticles in Polymer-Based Hybrid Composites", *Ibn AL-Haitham J. Pure Appl. Sci.*, 38(1) (2025) 186-196.

[25] I.A.H. Khudair, S.A.O. AL-Shiaa and M.K. Al-khaykanee, "Enhancing the Structural and Optical Properties of Poly (Vinyl Alcohol) Films Through the Incorporation of Ag_2O:ZnO Nanoparticle", *J. Compos. Adv. Mater. des Compos. des Matériaux Avancés*, 34(3) (2024) 349-355.

[26] O. Samson, T.O. Adeeko and E.K. Makama, "Synthesis and optical characterization of silver nanoparticles (Ag-NPs) thin films (TFs) prepared by silar technique", *Int. J. Curr. Res. Acad. Rev*, 5(12) (2017) 15-24.

[27] M.A.I. Molla et al., "Studies of effects of calcination temperature on the crystallinity and optical properties of Ag-doped ZnO nanocomposites", *J. Compos. Sci.*, 3(1) (2019) 18.

[28] R. Badry et al., "UV filters and high refractive index materials based on carboxymethyl cellulose sodium and CuO@ZnO core/shell nanoparticles", *Sci. Rep.*, 13(1) (2023) 21159.

[29] A. Atta et al., "Flexible methyl cellulose/polyaniline/silver composite films with enhanced linear and nonlinear optical properties", *Polymers (Basel)*, 13(8) (2021) 1225.

[30] S.Q. Abdul Hasan et al., "Studying the effect of the annealing on Ag_2Se thin film", *AIP Conf. Proc.*, 2307(1) (2020) 20007.

[31] K.A. Jasim, M.A.N. Thejeel and R.S. Al-Khafaji, "The Effect of Doping by Sr on the Structural, Mechanical and Electrical Characterization of $La_1Ba_{1-x}Sr_xCa_2Cu_4O_{8.5+\delta}$", *Ibn AL-Haitham J. Pure Appl. Sci.*, 27(1) (2017) 170-175.

[32] A.A. Barzinjy and B.S. Haji, "Green synthesis and characterization of Ag nanoparticles using fresh and dry Portulaca Oleracea leaf extracts: Enhancing light reflectance properties of ITO glass", *Micro Nano Lett.*, 19(3) (2024) e12198.

[33] A.K. Patel et al., "Synthesis and Characterization of CMC-Wrapped ZnONPs at Different Calcination Temperatures for Photocatalytic Degradation of Methylene Blue Dye under Sunlight", *J. Polym. Mater.*, 41(2) (2024) 69-86.

[34] A.A. Al-Shamari et al., "Structural and optical properties of PEO/CMC polymer blend modified with gold nanoparticles synthesized by laser ablation in water", *J. Mater. Res. Technol.*, 12 (2021) 1597-1605.

[35] R.S. Al-Khafaji and F.Q. Mohammed, "Effect of catalysts on BN NanoParticles production", *J. Mater. Res. Technol.*, 9(1) (2020) 868-874.

Table (2) FTIR spectrum data for the AgNPs and CMC

Sample	Position (cm^{-1})	Bond Type	Power	Vibration	Functional Group
Ag as-prepared	3343	O-H and N-H	strong	stretching	alcohol
	1637	C=C	medium	stretching	Conjugated alkene
	1248	C=O	strong	stretching	Alky aryl ether
Ag after Calcination 300°C	3372	O-H	strong	stretching	alcohol
	2889	C-H	medium	stretching	alkene
	1589	N-H	medium	bending	amine
	1340	O-H	medium	bending	alcohol
	1234	C=O	strong	stretching	Alky aryl ether
	893	C=C	strong	bending	alkene
CMC	3312	O-H	strong	stretching	alcohol
	2913	C-H	medium	stretching	alkene
	1590	C-C	medium	stretching	aromatics
	1372	O-H	medium	bending	alcohol
	1153	S=O	strong	stretching	sulfone
	897	C=C	strong	bending	alkene

• Strong bonds: Transmittance < 50%, • Medium bonds: Transmittance 50-70% and •Weak bonds: Transmittance > 70%

